

Reaction cross sections of carbon isotopes incident on a proton

B. Abu-Ibrahim,^{1,2} W. Horiuchi,³ A. Kohama,¹ and Y. Suzuki⁴

¹*RIKEN Nishina Center, RIKEN, Wako-shi, Saitama 351-0198, Japan*

²*Department of Physics, Cairo University, Giza 12613, Egypt*

³*Graduate School of Science and Technology, Niigata University, Niigata 950-2181, Japan*

⁴*Department of Physics, Graduate School of Science and Technology, Niigata University, Niigata 950-2181, Japan*

We systematically study total reaction cross sections of carbon isotopes with $N = 6-16$ on a proton target for wide range of incident energies, putting an emphasis on the difference from the case of a carbon target. The analysis includes the reaction cross sections of $^{19,20,22}\text{C}$ at 40 AMeV, the data of which have recently been measured at RIKEN. The Glauber theory is used to calculate the reaction cross sections. To describe the intrinsic structure of the carbon isotopes, we use a Slater determinant generated from a phenomenological mean-field potential, and construct the density distributions. To go beyond the simple mean-field model, we adopt two types of dynamical models: One is a core+ n model for odd-neutron nuclei, and the other is a core+ $n+n$ model for ^{16}C and ^{22}C . We propose empirical formulas which are useful in predicting unknown cross sections.

PACS numbers: 25.60.Dz, 21.10.Gv, 25.60.-t, 24.10.Ht

Keywords:

I. INTRODUCTION

Reactions of unstable neutron-rich nuclei with a proton target are of current interest [1, 2] since such reactions are at present the major means to sensitively probe the matter densities of exotic nuclei, especially the region of nuclear surface. If one appropriately selects incident energies, protons could be more sensitive to neutron distributions than proton distributions of nuclei.

The structure of carbon isotopes has recently attracted much attention. Several works have been done already experimentally [3, 4, 5, 6] and theoretically [7, 8, 9, 10, 11]. For example, the structure of ^{22}C has been studied by two (W.H. and Y.S.) of the present authors in a three-body model of $^{20}\text{C}+n+n$. They showed that it has a Borromean character [12].

The purpose of this paper is to report a systematic analysis of the total reaction cross sections of carbon isotopes incident on a proton at energies from 40 AMeV to 800 AMeV, and predict the cross sections of neutron-rich isotopes. We also estimate the cross sections contributed by protons or neutrons in the nuclei of carbon-isotopes. This study is motivated by an ongoing measurement of the reaction cross section of ^{22}C at RIKEN [13].

Recently, we have performed systematic analyses of total reaction cross sections of carbon isotopes on ^{12}C for wide energy range using the Glauber model [14]. We found reasonable parameterizations of nucleon-nucleon scattering amplitudes, and obtained fairly good agreement with available data. We predicted the total reaction cross section of a neutron-rich isotope, ^{22}C on ^{12}C , and obtained a sizable effect of the extended surface. Another purpose of this study is to discuss the advantage and disadvantage of a proton and a carbon target.

In this paper, we adopt the same prescription as our previous work [14] for describing the nuclear structure, and calculate the total reaction cross sections of proton-carbon isotopes similarly to the case of ^{12}C target. We

calculate systematically total reaction cross sections for wide energy range using the Glauber model. Of course, we should note that the model may not be so good at 40 AMeV.

We treat the interactions of proton-proton and proton-neutron separately. The wave functions of carbon isotopes are generated based on a simple mean-field model. To go beyond that, we adopt two types of dynamical models: One is a core+ n model for an odd N nucleus, and the other is a core+ $n+n$ model for ^{16}C and ^{22}C . The reason for the latter model is explained in Ref. [14]. We do not take into account the Coulomb potential, which would affect the magnitude of the cross sections for the low energy processes to some extent, but, for the present discussion, the effect is minor.

This paper is organized as follows: The reaction models for the calculations of reaction cross sections are presented in Sec. II. We explain our input data in Sec. III. We present the cross section calculation in Sec. IV. The contributions of the protons and neutrons inside an isotope to the reaction cross section are presented in Sec. V. Summary is given in Sec. VI. In Appendix, we discuss the parameterization of the nucleon-nucleon scattering amplitude.

II. THE GLAUBER MODEL FOR REACTION CROSS SECTION CALCULATIONS

Here we summarize our basic formula for the following discussions.

The total reaction cross section of proton-nucleus collisions is expressed as

$$\sigma_R = \int d\mathbf{b} \left(1 - |e^{i\chi(\mathbf{b})}|^2\right), \quad (1)$$

where \mathbf{b} is the impact parameter vector perpendicular to the beam (z) direction, and $\chi(\mathbf{b})$ is the phase-shift

function defined below. We calculate this quantity using the Glauber theory.

The Glauber theory provides us with an excellent framework to describe high energy reactions. In this framework, the optical phase-shift function (the elastic S -matrix) for proton-nucleus scattering is given by [15]

$$e^{i\chi(\mathbf{b})} = \langle \psi_0 | \prod_{i=1}^A \left[1 - \frac{1 + \tau_{3i}}{2} \Gamma_{pn}(\mathbf{b} + \mathbf{s}_i) - \frac{1 - \tau_{3i}}{2} \Gamma_{pp}(\mathbf{b} + \mathbf{s}_i) \right] | \psi_0 \rangle, \quad (2)$$

where ψ_0 is the intrinsic (translation-invariant) A -nucleon wave function of the projectile's ground state (A is the mass number of the projectile), and \mathbf{s}_i is the projection onto the xy -plane of the nucleon coordinate relative to the center-of-mass of the projectile. Here τ_{3i} is 1 for neutron and -1 for proton.

When we apply this framework to low energy processes, such as the one less than 100 MeV, its usefulness should be carefully assessed. As a prescription, we carefully choose the parameters of the nucleon-nucleon scattering amplitude so as to reproduce the reaction cross sections of proton- ^{12}C scatterings in consistent with those of ^{12}C - ^{12}C scatterings [14].

The profile function, Γ_{pN} , for pp and pn scatterings, is usually parameterized in the form;

$$\Gamma_{pN}(\mathbf{b}) = \frac{1 - i\alpha_{pN}}{4\pi\beta_{pN}} \sigma_{pN}^{\text{tot}} e^{-b^2/(2\beta_{pN})}, \quad (3)$$

where α_{pN} is the ratio of the real to the imaginary part of the pp (pn) scattering amplitude in the forward direction, σ_{pN}^{tot} is the pp (pn) total cross sections, and β_{pN} is the slope parameter of the pp (pn) elastic scattering differential cross section. We parameterize the nucleon-nucleon scattering amplitude with a single Gaussian, because we find that double Gaussians give numerically almost the same reaction cross sections as the single Gaussian. We discuss this point in Appendix.

There are several approximate expressions of the Glauber model on the market. We explain some of the expressions below.

In the optical limit approximation (OLA), the phase-shift function of proton-nucleus scattering is given by

$$e^{i\chi_{\text{OLA}}(\mathbf{b})} = \exp[i\chi_n(\mathbf{b}) + i\chi_p(\mathbf{b})], \quad (4)$$

with

$$\begin{aligned} i\chi_p(\mathbf{b}) &= -\int d\mathbf{r} \rho_p(\mathbf{r}) \Gamma_{pp}(\mathbf{s} + \mathbf{b}), \\ i\chi_n(\mathbf{b}) &= -\int d\mathbf{r} \rho_n(\mathbf{r}) \Gamma_{pn}(\mathbf{s} + \mathbf{b}), \end{aligned} \quad (5)$$

where χ_p (χ_n) implies the phase shift due to the protons (neutrons) inside the nucleus. The function $\rho_p(\mathbf{r})$ is the proton density distribution, and $\rho_n(\mathbf{r})$ is the neutron density.

In the few-body (FB) calculation, the OLA is used for the integration involving the coordinates of the core nucleons, while the integration for the valence-nucleon coordinate is performed without any approximation [16, 17, 18, 19]. In this treatment, Eq. (2) is reduced to the following expression for the case of core+ n configuration:

$$e^{i\chi_{\text{FB}}(\mathbf{b})} = \langle \varphi_0 | e^{i\chi_{Cp}(\mathbf{b}_C) + i\chi_{pn}(\mathbf{b}_C + \mathbf{s})} | \varphi_0 \rangle, \quad (6)$$

with

$$\mathbf{b}_C = \mathbf{b} - \frac{1}{A} \mathbf{s}, \quad (7)$$

where φ_0 is the single-particle wave function of the valence nucleon and \mathbf{b}_C is the impact parameter between the proton and the core. The phase-shift function, χ_{Cp} , of the proton-core scattering is defined in exactly the same way as Eq. (4). The proton-neutron phase-shift function, χ_{pn} , is defined through the relation; $\exp(i\chi_{pn}(\mathbf{b})) = 1 - \Gamma_{pn}(\mathbf{b})$. In this paper, we adopt both Eqs. (4) and (6) to calculate the phase-shift function.

In the discussion below, we adopt the kinematics of the projectile's rest frame. We specify processes by the energy of an incident proton. For example, the energy of 40 A MeV of an incident nucleus of the mass number A in the proton-fixed frame corresponds to the energy of 40 MeV of an incident proton in the projectile's rest frame.

III. INPUT DATA

In this section, we list the input quantities in the calculations of the reaction cross sections, and give some discussions.

The inputs for Eq. (2) are the projectile's intrinsic A -nucleon wave function and the parameters of the pp and pn profile functions. For Eq. (4), we need only proton and neutron intrinsic densities and the parameters of the profile functions. For Eq. (6), we need the single-particle wave function for the valence neutron as well.

The parameters of Γ_{pp} and Γ_{pn} are taken from Refs. [20, 21]. In Ref. [20], the experimental values of σ_{pp} , σ_{pn} , α_{pp} and α_{pn} are listed in energy range from 20 MeV to 300 MeV.

The parameters β_{pp} and β_{pn} are determined from the fact that the total elastic cross section, σ_{pN}^{el} , is equal to the total cross section in this energy range, since only the elastic scattering is energetically possible until the pion production threshold is open. For the profile function, Eq. (3), we have [17]

$$\sigma_{pN}^{\text{el}} = \frac{1 + \alpha_{pN}^2}{16\pi\beta_{pN}} (\sigma_{pN}^{\text{tot}})^2. \quad (8)$$

Since $\sigma_{pN}^{\text{el}} = \sigma_{pN}^{\text{tot}}$, we can derive the following expression for β_{pN} ;

$$\beta_{pN} = \frac{1 + \alpha_{pN}^2}{16\pi} \sigma_{pN}^{\text{tot}}. \quad (9)$$

The experimental data of Ref. [20] and the β_{pN} values determined from Eq. (9) are listed in Table I. In Ref. [21], all the needed parameters are listed in the energy range from 100 MeV to 1000 MeV. They are also given in Table I. For the energy higher than 300 MeV, β_{pN} is determined from Eq. (8) using both the data of σ_{pN}^{el} and σ_{pN}^{tot} . The data on σ_{pN}^{el} are taken from PDG tabulation [22] and the uncertainty of the data is fairly large.

As we show in Appendix, the description of the pn elastic differential cross section with these parameters is reasonable, but not perfect especially in the forward direction. Fortunately, this does not affect the total reaction cross sections. We discuss it in some detail in the appendix.

The densities that we use here are constructed from a core+ n model for the odd isotopes, $^{13,15,17,19}\text{C}$, where the cores are $^{12,14,16,18}\text{C}$, respectively. For $^{16,22}\text{C}$, a core+ $2n$ model is assumed. The densities of the carbon isotopes are displayed in Fig. 1, and the corresponding root-mean-square (rms) radii are summarized in Table II. The detail of these densities can be found in Ref. [14].

IV. PREDICTION OF THE REACTION CROSS SECTIONS

Here we show our numerical results of the total reaction cross sections of proton-carbon isotopes reactions.

Before we predict the reaction cross sections for the isotopes, we first show how well our densities and the pa-

TABLE I: Parameters of the pn and pp profile functions as defined in Eq. (3). E is the projectile's incident energy.

E (MeV)	σ_{pp}^{tot} (fm ²)	α_{pp}	β_{pp} (fm ²)	σ_{pn}^{tot} (fm ²)	α_{pn}	β_{pn} (fm ²)
40	7.0	1.328	0.385	21.8	0.493	0.539
60	4.7	1.626	0.341	13.6	0.719	0.410
80	3.69	1.783	0.307	9.89	0.864	0.344
100	3.16	1.808	0.268	7.87	0.933	0.293
120	2.85	1.754	0.231	6.63	0.94	0.248
140	2.65	1.644	0.195	5.82	0.902	0.210
160	2.52	1.509	0.164	5.26	0.856	0.181
180	2.43	1.365	0.138	4.85	0.77	0.154
200	2.36	1.221	0.117	4.54	0.701	0.135
240	2.28	0.944	0.086	4.13	0.541	0.106
300	2.42	0.626	0.067	3.7	0.326	0.081
425	2.7	0.47	0.078	3.32	0.25	0.0702
550	3.44	0.32	0.11	3.5	-0.24	0.0859
650	4.13	0.16	0.148	3.74	-0.35	0.112
700	4.43	0.1	0.16	3.77	-0.38	0.12
800	4.59	0.06	0.185	3.88	-0.2	0.12
1000	4.63	-0.09	0.193	3.88	-0.46	0.151

rameters of the profile functions fit the experimental data of the proton- ^{12}C total reaction cross sections. In Fig. 2, we compare the numerical results with the experimental data over the energy range from 40 MeV to 800 MeV. As one can see from the figure, they reasonably agree with each other over all the energy range. At energies lower than 100 MeV, where the data fluctuate by 15 % at most, our results follow the largest data. In this energy region, a systematic uncertainty of our approach is estimated to be about 15 %, which is consistent with the estimation by two of us (B.A.-I. and Y.S.) for the case of $^6\text{He}+^{12}\text{C}$ reaction 40 AMeV [23]. They confirmed that the eikonal approximation gives about 15 % larger cross sections than those by the quantum-mechanical (exact) calculation.

Now we show our predictions for all the carbon isotopes at all the energies using the parameters given in Table I. The numerical results of the total reaction cross sections are summarized in Table III.

Let us estimate the contributions of the breakup effect although it is expected to be small for a proton target. Equations (2) and (6) contain the breakup effect, while Eq. (4) does not. We compare them to estimate the breakup effect. As an illustrative example, we calculate the reaction cross section of a typical halo nucleus, ^{19}C , incident on a proton using Eqs. (4) and (6). We assume the structure of ^{19}C as $^{18}\text{C}+n$ with the one-neutron separation energy of 0.581 MeV [24]. The numerical results at 40 MeV and 800 MeV are 763 mb (758 mb) and 372 mb (373 mb) respectively when Eq. (6) (Eq. (4)) is used. The difference is less than one %, which is consistent with the results of Ref. [16]. The breakup effect can therefore be neglected. This validates our use of Eq. (4).

For convenience, we introduce the black-sphere radius, a , defined through [25]

$$\sigma_{\text{R}} = \pi a^2. \quad (10)$$

Following the Carlson's prescription [26], we fit the numerical results by parameterizing the radius, a , using a

TABLE II: The rms radii in fm of matter, neutron and proton density distributions for the carbon isotopes.

Isotopes	r_m	r_n	r_p
^{12}C	2.31	2.30	2.33
^{13}C	2.37	2.40	2.34
^{14}C	2.39	2.46	2.31
^{15}C	2.65	2.84	2.34
^{16}C	2.66	2.83	2.34
^{17}C	2.94	3.20	2.38
^{18}C	2.78	2.96	2.36
^{19}C	3.09	3.37	2.38
^{20}C	2.99	3.23	2.37
^{22}C	3.58	3.92	2.43

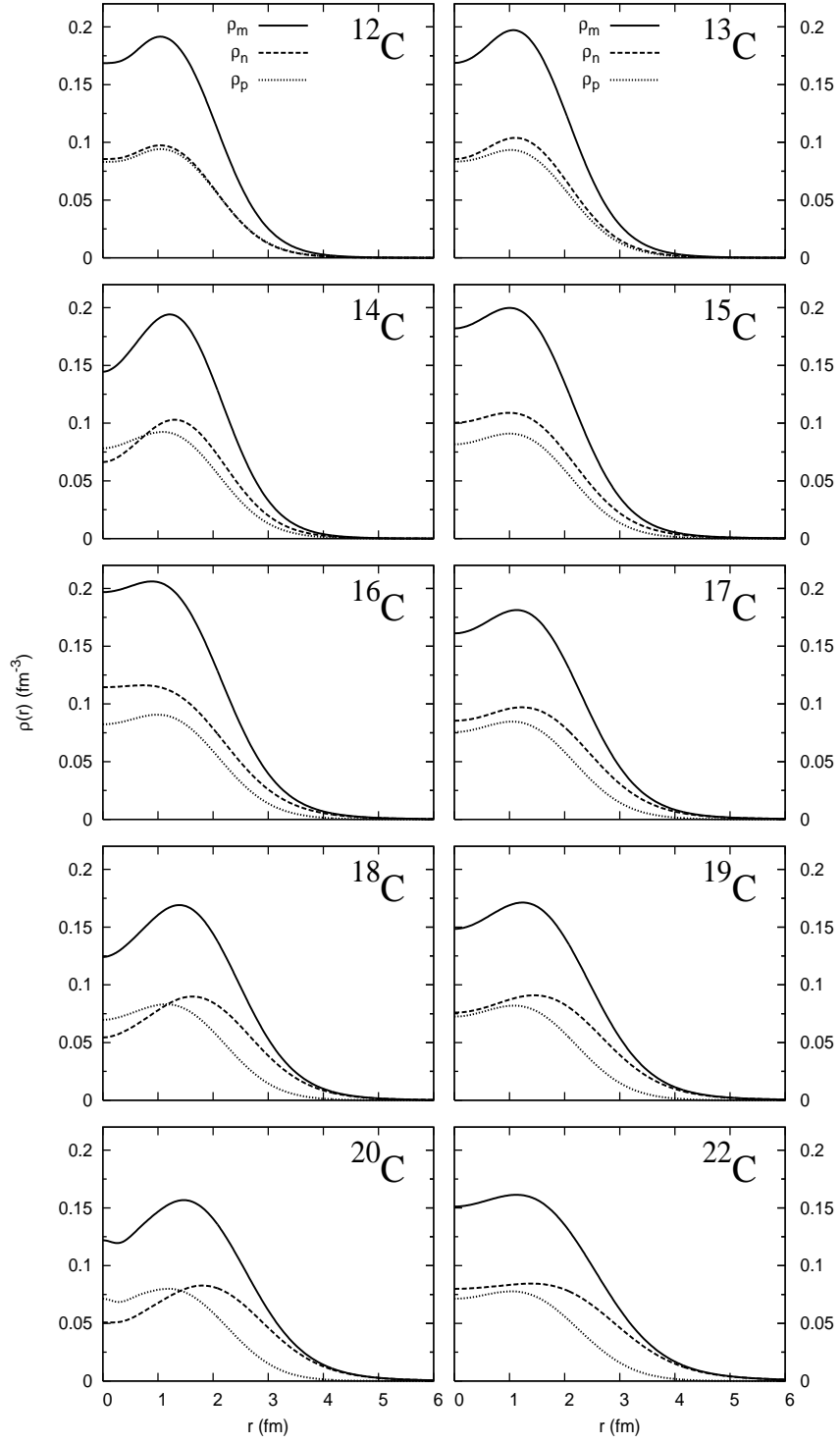


FIG. 1: Density distributions of the carbon isotopes. The dotted curve shows the proton density, the dashed curve the neutron density, and the solid curve the matter density.

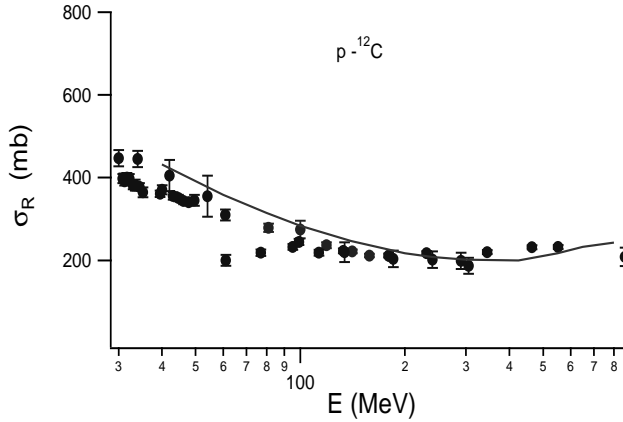


FIG. 2: Comparison of the numerical results with the experimental data for the total reaction cross sections of proton- ^{12}C reaction as a function of energy. The experimental data are taken from Refs. [26, 27].

TABLE III: Total reaction cross sections of proton-carbon isotopes in units of mb. E is the projectile's incident energy.

E (MeV)	Isotopes										
	^{12}C	^{13}C	^{14}C	^{15}C	^{16}C	^{17}C	^{18}C	^{19}C	^{20}C	^{22}C	
40	432	467	489	580	605	682	662	758	761	957	
100	284	308	327	372	394	436	443	491	509	604	
200	218	236	252	282	300	330	340	372	390	453	
300	202	218	231	257	273	299	309	337	353	407	
425	200	214	227	251	265	289	300	324	339	389	
550	217	231	242	267	282	307	315	341	356	408	
650	233	247	259	284	299	324	332	359	374	429	
800	243	257	268	294	309	335	342	373	385	442	

simple geometric picture with a correction term;

$$a = C_0 + r_0 A^{1/3}. \quad (11)$$

This includes a $A^{1/3}$ correction in addition to the simple geometrical $A^{2/3}$ term. In Ref. [26], Carlson used R_p instead of C_0 here. He fitted the reaction cross sections of stable nuclei incident on a proton target in the energy range from 40 MeV to 560 MeV.

In Fig. 3, we compare our numerical results (open circles) listed in Table III with the fit using Eq. (11) (solid lines) at 40, 100 and 550 MeV. The values of C_0 and r_0 extracted from the fit are given in Table IV. These values that we find are different from those obtained by Carlson, which are given in the parentheses in the table.

The parameter C_0 implies the strength of $A^{1/3}$ correction to $A^{2/3}$ -dependence of the reaction cross sections. The values in Table IV decrease with the energy, which is consistent with the geometrical picture of the cross section at high energy, because $\sigma_R \propto A^{2/3}$ for proton-nucleus reaction.

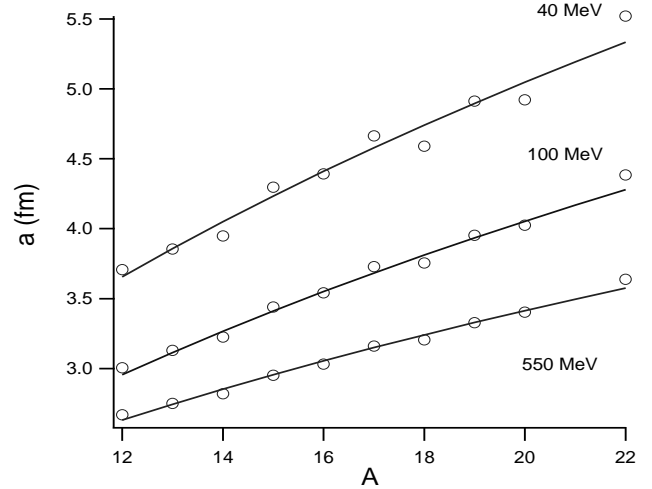


FIG. 3: Comparison of the black square radii, $a = \sqrt{\sigma_R/\pi}$, for the numerical results of the carbon isotopes (open circles) with the fit using Eq. (11) (solid line) as a function of the mass number.

As one can see from Fig. 3, the curves with our parameters nicely fits the numerical results for the stable isotopes as well as the neutron-rich unstable isotopes. The estimations with Carlson's parameters underestimates our numerical results for neutron-rich cases. This reflects an anomalous mass number dependence of the size of such exotic nuclei. Even with the new parameterization, the reaction cross section of ^{22}C is even larger than the fit, especially at 40 MeV. This would suggest an extended surface structure of ^{22}C . We believe that this simple fitting formula will serve as a reference for discussions of the total reaction cross sections.

Moreover, we empirically deduce the rms nuclear matter radii, using the black-sphere radius, a , of Eq. (10). If we assume a rectangular density distribution for nuclei, we obtain

$$r_{\text{BS}} = \sqrt{\frac{3}{5}} a = \sqrt{\frac{3}{5}} \sqrt{\frac{\sigma_R}{\pi}}. \quad (12)$$

This radius clearly depends on the incident energy. At around 100 MeV, this r_{BS} value happens to agree reasonably well with r_m listed in Table II. This suggests that we may empirically access to the rms nuclear matter radii of carbon isotopes just by measuring σ_R at 100 MeV. This is consistent with the estimations in Ref. [25]. The authors of Ref. [25] pointed out that, for $T_p \gtrsim 800$ MeV, r_{BS} almost completely agrees with the empirically deduced values of the rms matter radius for stable nuclei having mass $A \gtrsim 50$, while it systematically deviates from the deduced values for $A \lesssim 50$ [25]. Since carbon isotopes belong to light nuclei, we may choose the energy which gives a little bit larger σ_R to obtain r_{BS} close to r_m .

We propose another empirical formula. For all the carbon isotopes, we find that the following relation is satis-

fied over all the energy range:

$$\frac{\sigma_R(p + {}^{6+N}_6\text{C})}{\sigma_R(p + {}^{12}_6\text{C})} = R(C) \frac{6\sigma_{pp}^{\text{tot}} + N\sigma_{pn}^{\text{tot}}}{6\sigma_{pp}^{\text{tot}} + 6\sigma_{pn}^{\text{tot}}}, \quad (13)$$

with $R(C) = 0.96 \pm 0.05$. Here $N \geq 7$ and $\sigma_{pp}^{\text{tot}}(\sigma_{pn}^{\text{tot}})$ is the proton-proton (proton-neutron) total cross section at a given energy. The value of $R(C)$ is obtained by averaging the 153 numerical results (9 isotopes times 17 energy points) of the reaction cross sections, and 0.05 is the standard deviation of these points. At high energy, $R(C)$ of Eq. (13) is very close to unity. In Fig. 4, we plot $R(C)$ for selected energies. Only at 40 MeV, some points come slightly below this relation, which would suggest the breakdown of the approximations, such as the fixed-scatterer approximation, contained in the Glauber model.

At least for carbon isotopes, the expression (13) indicates that if we know the reaction cross section of a stable isotope, we can predict the reaction cross section of other isotope within the error bar. Whether this holds for any nuclides or not is left for a future study.

Experimental data are expected to appear at around 40 MeV for ${}^{19,20,22}\text{C}$ [13]. Here we predict them. In Fig. 5, we compare our prediction for the reaction cross sections of carbon isotopes with the available experimental data. The preliminary data of proton- ${}^{22}\text{C}$ reaction cross section has been reported to be around 1000 mb with a large uncertainty [13], which is consistent with our prediction.

For ${}^{22}\text{C}$, we generate several densities that give different two-neutron separation energies of 0.489, 0.361, 0.232 and 0.122 MeV for the last two neutrons. All of them lie within the error bar of the experimental value, 0.423 ± 1.140 MeV [24]. Using these densities, we calculate the reaction cross sections for proton- ${}^{22}\text{C}$ reaction at 40 MeV in order to examine the separation-energy dependence. The results are listed in Table V. The change in radius from 3.6 to 4.1 fm gives change in the reaction

cross section of about 50 mb at 40 MeV. At 800 MeV, the change in the reaction cross section is about 10 mb. This gives an estimate of an uncertainty of our calculations.

V. THE NEUTRON CONTRIBUTION TO THE REACTION CROSS SECTION

Here we estimate that contribution to reaction cross sections which comes from the neutrons in the nucleus. Reactions with a proton are superior to those with a ${}^{12}\text{C}$ when we look into such separate contributions, because ${}^{12}\text{C}$ is equally sensitive to protons and neutrons. For the purpose of discussion here, we use the following relation:

$$\begin{aligned} 1 - |e^{i\chi_n(b)+i\chi_p(b)}|^2 &= |e^{i\chi_p(b)}|^2 \left(1 - |e^{i\chi_n(b)}|^2\right) \\ &+ |e^{i\chi_n(b)}|^2 \left(1 - |e^{i\chi_p(b)}|^2\right) \\ &+ \left(1 - |e^{i\chi_n(b)}|^2\right) \left(1 - |e^{i\chi_p(b)}|^2\right). \end{aligned} \quad (14)$$

Then we define the proton-nucleus reaction probability $P_A(b)$ and its decomposition into neutron and proton contributions, $P_n(b)$ and $P_p(b)$, as

$$P_A(b) = P_n(b) + P_p(b), \quad (15)$$

where

$$\begin{aligned} P_n(b) &= |e^{i\chi_p(b)}|^2 \left(1 - |e^{i\chi_n(b)}|^2\right) \\ &+ c \left(1 - |e^{i\chi_n(b)}|^2\right) \left(1 - |e^{i\chi_p(b)}|^2\right), \\ P_p(b) &= |e^{i\chi_n(b)}|^2 \left(1 - |e^{i\chi_p(b)}|^2\right) \\ &+ d \left(1 - |e^{i\chi_n(b)}|^2\right) \left(1 - |e^{i\chi_p(b)}|^2\right), \end{aligned} \quad (16)$$

where $c + d = 1$, and c and d represent the neutron and proton contributions from the interference term, respectively. Equation (1) is expressed as

$$\sigma_R = 2\pi \int_0^\infty b db P_A(b). \quad (17)$$

TABLE IV: The parameters of Eq. (11) which give the lines plotted in Fig. 3. The values in the parentheses are those of Carlson [26].

E (MeV)	C_0 (fm)	r_0 (fm)
40	-3.83 (1.00)	3.27 (1.21)
80	-3.123	2.73
100	-2.95 (-0.31)	2.58 (1.37)
140	-2.68	2.38
200	-2.46	2.21
240	-2.36	2.14
300	-2.14	2.03
425	-1.62	1.85
550	-1.58 (-0.30)	1.84 (1.33)
800	-1.31	1.782

TABLE V: The reaction cross sections of ${}^{22}\text{C}$ incident on a proton target at 40 AMeV for different two-neutron separation energies, S_{2n} . The r_m value denotes the rms matter radius.

S_{2n} (MeV)	r_m (fm)	σ_R (mb)
0.489	3.6	957
0.361	3.7	969
0.232	3.8	985
0.122	4.1	1005

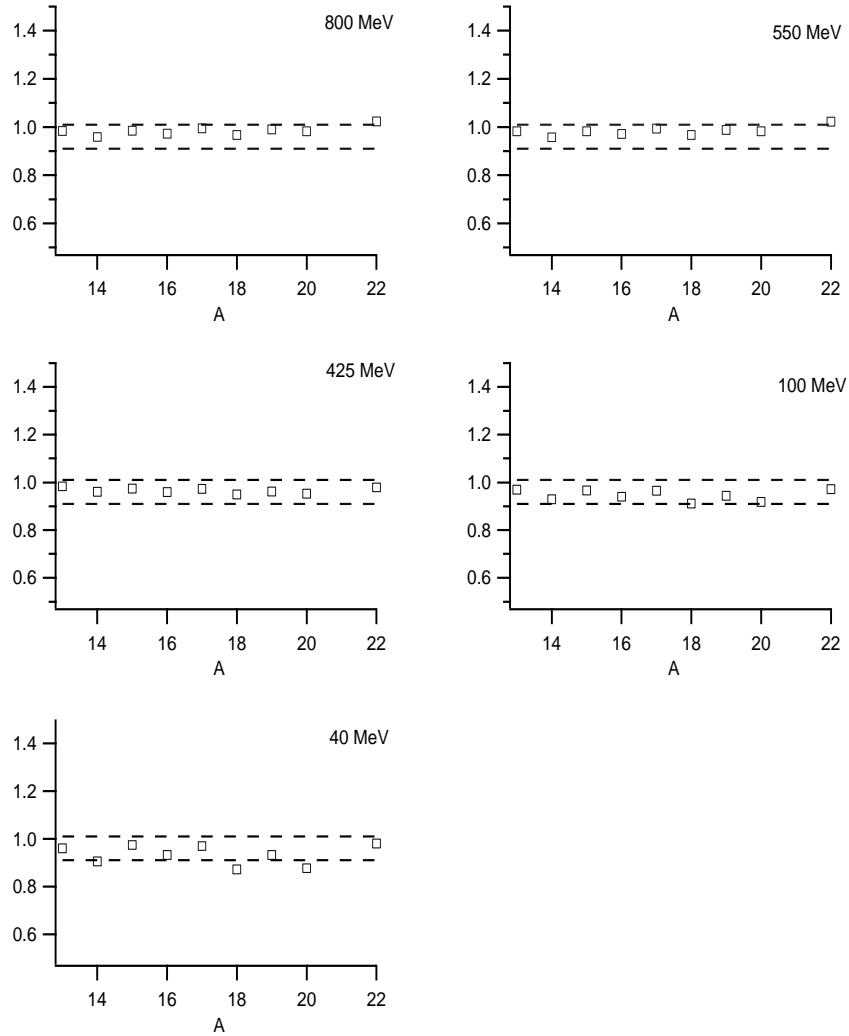


FIG. 4: The values of $R(C)$ of Eq. (13) as a function of the mass number, A . The dashed lines denote 0.96 ± 0.05 values.

The values of c and d must satisfy the condition, $c + d = 1$, but the choice of them is not unique. Here we discuss two cases; 1) $c = d = 1/2$, 2) $c = N/A$ and $d = Z/A$, to see the dependence of the choice. The former implies that both neutrons and protons contribute equally to the interference term, while the latter implies that the contribution of the neutrons and protons to the interference term is proportional to their numbers.

In Fig. 6, we show our predictions of the total reaction cross section of proton- ^{22}C reaction as a function of energy (solid curve). We also draw the neutron and proton contributions for $c = d = 1/2$ (dash-dot-dotted and dash-dotted) and $c = N/A$, $d = Z/A$ (dashed and dotted), respectively. Due to the fact that ^{22}C is very neutron-rich, we learn from this figure that the neutron contribution dominates the reaction cross sections. Also we find that the proton and neutron contributions depend modestly on the choice of the values of c and d . For example, for $c = d = 1/2$, the neutron

contribution to the total reaction cross section of ^{22}C , $2\pi \int_0^\infty b db P_n(b) / 2\pi \int_0^\infty b db P_A(b)$, is about 0.87 and 0.73 at 40 MeV and 800 MeV, respectively. For $c = N/A$, $d = Z/A$, the neutron contribution to the total reaction cross sections is about 0.93 and 0.80 at 40 MeV and 800 MeV, respectively.

According to Eq. (13), the neutron contribution to the total reaction cross section would be similar to the ratio $N\sigma_{pn}^{\text{tot}} / (Z\sigma_{pp}^{\text{tot}} + N\sigma_{pn}^{\text{tot}})$. At 40 MeV and 800 MeV, the ratio of $N\sigma_{pn}^{\text{tot}} / (Z\sigma_{pp}^{\text{tot}} + N\sigma_{pn}^{\text{tot}})$ reads 0.89 and 0.69, respectively. These values are quite similar to the above ratios of our numerical results.

Figure 7 shows the reaction probability times $2\pi b$ of proton- ^{12}C reaction as a function of the impact parameter, b . We plot $2\pi b P(b)$, because this quantity more directly reflects the contribution to σ_R than $P(b)$ itself. The solid curve represents the total reaction probability, $P_A(b)$, in Eq. (15). The neutron contribution $P_n(b)$ is shown by the dashed curve and the proton contribution

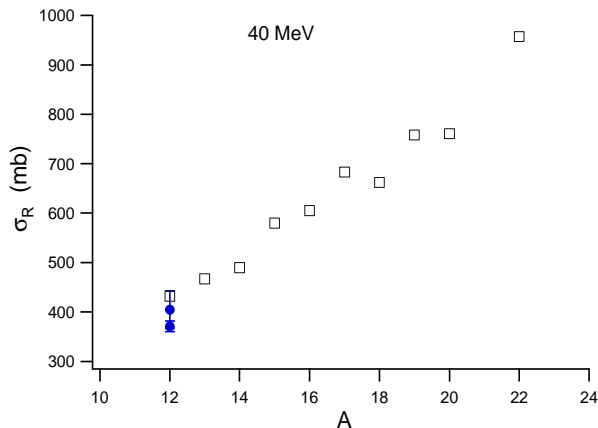


FIG. 5: Reaction cross section for the carbon isotopes at 40 MeV. The experimental data are taken from Ref. [26]. The larger one is natural carbon at 42 MeV, and the smaller one is ^{12}C at 40 MeV. The energy is converted to the case of a proton target. The preliminary data for ^{22}C is about 1000 mb with a large uncertainty [13].

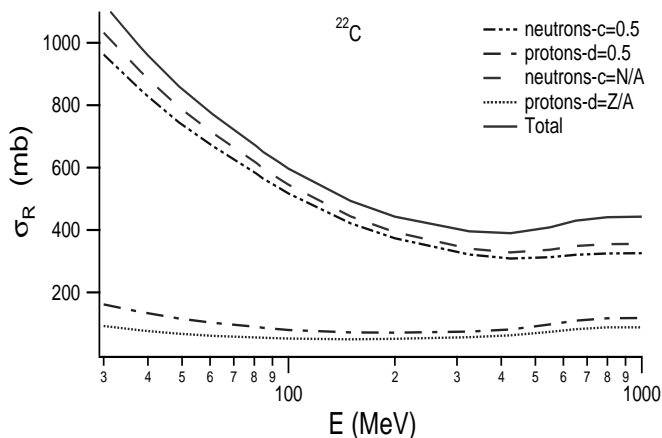


FIG. 6: The total reaction cross section of proton- ^{22}C as a function of energy (solid curve), and its decomposition to the neutron and proton contributions.

$P_p(b)$ is shown by the dotted curve. Here we draw only the case of $c = d = 1/2$. One can see from the figure that, at 40 MeV, the neutron contribution to the total reaction probability is about two times of the proton contribution, while at 800 MeV the proton contribution exceeds that of the neutron. This reflects the behavior that the pn total cross section, σ_{pn}^{tot} , is significantly larger than the pp total cross section, σ_{pp}^{tot} , at low energy region.

Figure 8 displays the reaction probability of proton- ^{22}C reaction, similarly to that of proton- ^{12}C reaction. In contrast to the case of ^{12}C , the neutron contribution to the reaction probability is larger than that of the proton over all the energy range. Also, the reaction probability on the surface region comes mostly from the neutron contribution at all the energy range. This is due to the

large extension of the neutron density, as shown in Fig. 1.

The difference between the reaction probability of proton- ^{12}C and that of proton- ^{22}C is as follows: Let the probing position of the proton be an impact parameter at which $2\pi bP(b)$ becomes a maximum. The probing position for the case of proton- ^{12}C at 800 MeV is at 2.0 fm, and the maximum height is about 10 fm, while they are about 2.7 fm and 13 fm in the case of ^{22}C . The reaction probability of proton- ^{12}C at 800 MeV reaches zero at about 6 fm, while in the case of proton- ^{22}C it reaches zero at about 10 fm. The major contribution comes from the region around the probing point, *i.e.*, the surface.

In order to compare the sensitivity of the proton and carbon probes to the nuclear surface, we plot, in Fig. 9, $\sigma_R(b)/\sigma_R$ for three nuclei, ^{12}C , ^{19}C and ^{22}C , of different features as a function of the impact parameter, b , where $\sigma_R(b)$ is defined similarly to Eq. (1) but the upper limit of the integration is limited to b . The nucleus ^{12}C is a stable nucleus which has almost the same proton and neutron distributions, ^{19}C is a good example of one-neutron halo nucleus, whereas ^{22}C is a two-neutron halo nucleus with a long neutron tail.

As one can see from the figures, for each case, the major contribution comes from the surface region, which supports the above discussion. As a rough estimate of the extent to which the surface region is probed, we may use an impact parameter at which $\sigma_R(b)$ reaches 90 % of σ_R . Then we take the difference of such impact parameters, Δb , between 40 and 800 MeV incident energies. The increase of Δb for the change of incident energy from 800 to 40 MeV is understood from the fact that the pn interaction becomes longer-ranged and stronger, which is reflected in the energy-dependence of β_{pn} and σ_{pn}^{tot} .

First we focus on the reaction cross sections for the proton target. The Δb value increases from 0.6, 1.5 to 1.9 fm as the neutron density becomes more widely distributed for ^{12}C , ^{19}C and ^{22}C , respectively. This suggests that the proton target can probe the density distribution near the surface up to further distances as the interaction range increases. The corresponding Δb value for the ^{12}C target case is 0.7, 1.3 and 1.6 fm for ^{12}C , ^{19}C and ^{22}C , respectively. Comparing Δb values for the proton targets with those for ^{12}C targets, we can conclude that the ^{12}C target can probe the surface region equally to the proton target but is disadvantageous to probe the remote surface region of the spatially extended neutron distribution, such as ^{22}C , compared to the proton. This is due to the fact that the proton and neutron distributions in ^{12}C are very similar and that the $nn(pp)$ interaction is shorter-ranged and weaker than the pn interaction.

It would be possible to probe the outer region of the density distribution by the proton target especially at lower energy, but, at very low energy, we have to note that the long wavelength of the proton leads to a low resolution to the resultant density distributions, which may prevent us from studying minute structures of the outer density in detail.

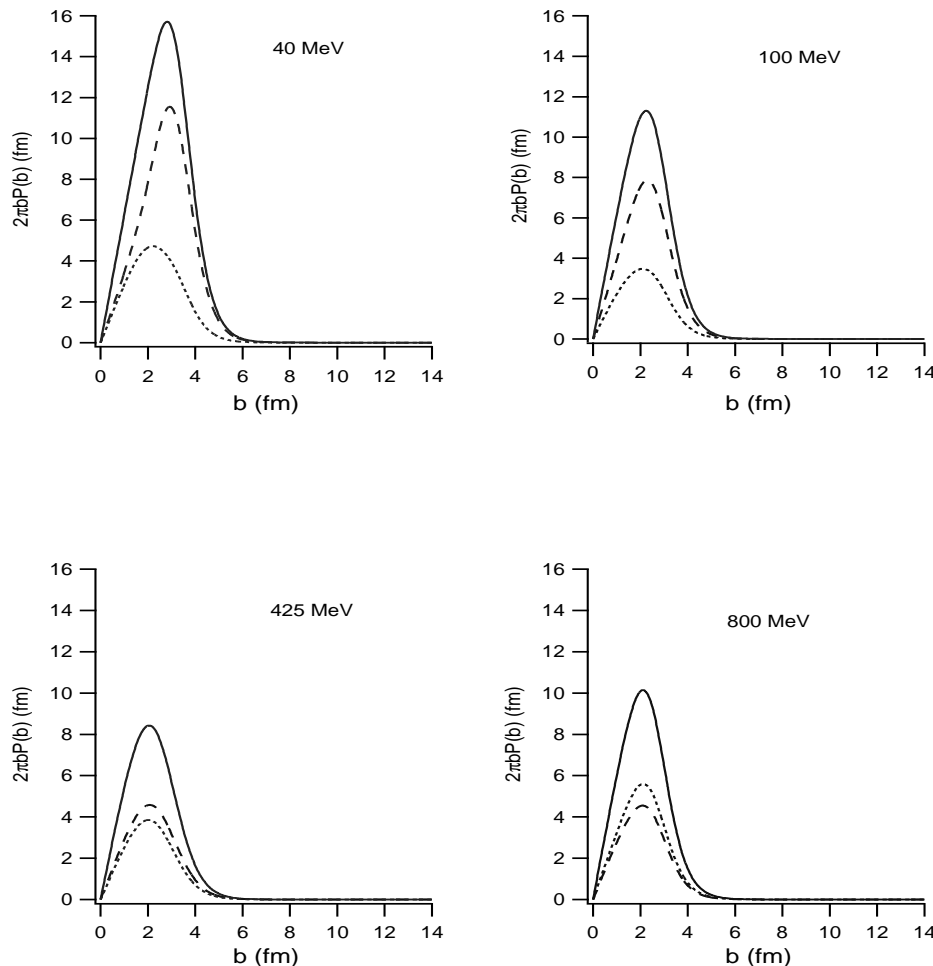


FIG. 7: Reaction probability, Eq. (16), times $2\pi b$ for proton- ^{12}C . The solid curve is the total probability. The dashed curve is the neutron contribution, while the dotted curve is the proton contribution. The choice of $c = d = 1/2$ is made.

VI. SUMMARY

We have made a systematic analysis of the total reaction cross sections for the carbon isotopes incident on a proton target for wide energy range, in comparison with the features of a carbon target. We have predicted the reaction cross sections especially at 40 MeV where the experimental data have been measured at RIKEN.

We have formulated this problem using the Glauber theory. The inputs are the parameters of nucleon-nucleon profile functions and the wave functions (densities) of carbon isotopes. The parameters of the nucleon-nucleon scattering are determined from the available experimental data. The densities are generated using the wave functions of the Slater determinant, which we used in our previous work [14]. To go beyond that, we use a core+ n model for odd nuclei and a core+ $n+n$ model for $^{16,22}\text{C}$ nuclei.

Having treated the interactions of proton-proton and proton-neutron separately, we have shown that the optical limit approximation of the Glauber theory gives al-

most the same results as the few-body calculation for the proton-nucleus reaction cross section over all the energy range used here.

For ^{22}C , we generate several densities which are constructed from the wave functions giving different separation energies of 0.489, 0.361, 0.232 and 0.122 MeV for the last two neutrons. All of them lie within the error bar of the experimental value, 0.423 ± 1.140 MeV. The reaction cross sections calculated using these densities are 957, 969, 985 and 1005 mb, respectively, for proton- ^{22}C at 40 MeV. Since the preliminary data of proton- ^{22}C reaction cross section has been reported to be around 1000 mb with a large uncertainty, all of our predictions are consistent with the data, but the larger two values, 985 and 1005 mb, would be favorable. If so, the data may suggest very small S_{2n} .

At around 100 MeV, the values of r_{BS} defined by Eq. (12) happen to agree reasonably well with r_m listed in Table II, which suggests that we may empirically access to the rms nuclear matter radii of carbon isotopes just by measuring σ_{R} at 100 MeV.

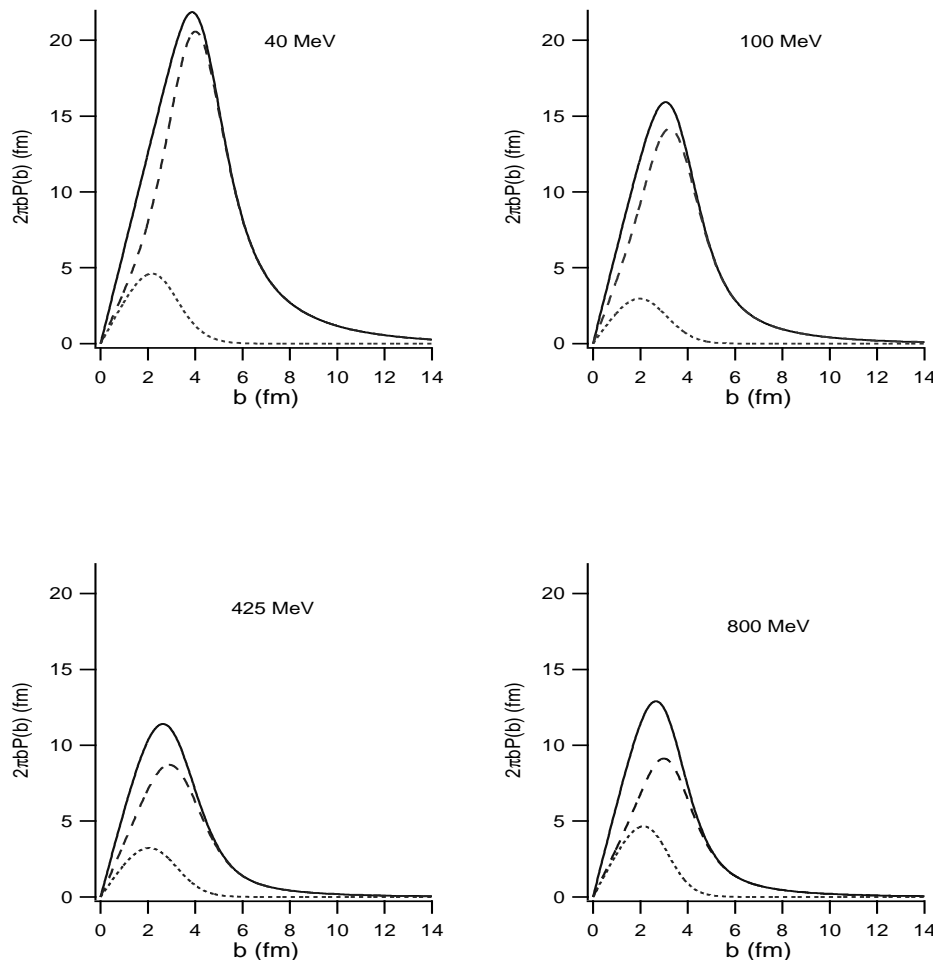


FIG. 8: The same as in Fig. 7 but for proton- ^{22}C case. The choice of $c = d = 1/2$ is made.

We have found a parameter free new relation, Eq. (13). It helps us to predict reaction cross sections for various isotopes at a given energy if the reaction cross section value of some stable isotope is available.

Finally, we have made simple estimates for the contribution of the neutron and the proton to the total reaction cross sections. The major contribution to σ_R comes from the surface region. Moreover, we have pointed out that a proton target can probe the surface region of the neutron-rich nuclei better than a ^{12}C target especially at lower incident energy.

We acknowledge T. Motobayashi for his encouragement during the course of this work. W. H. is a Research Fellow of the Japan Society for the Promotion of Science for Young Scientists. A. K. would like to thank K. Iida, K. Oyamatsu, and M. Takashina for useful comments and helpful discussions. This work was in part supported by a Grant for Promotion of Niigata University Research Projects (2005–2007), and a Grant-in Aid for Scientific Research for Young Scientists (No. 19-3978). One of the authors (Y.S.) thanks the JSPS core-to-core program,

Exotic Femto Systems.

Appendix: NN Scattering Amplitudes

Here we discuss the parameterizations of nucleon-nucleon scattering amplitudes. In the text, we parameterize it with a single Gaussian. We show here that the parameterization with double Gaussians gives numerically almost the same results for the reaction cross sections as the single Gaussian, and validates our use of the single Gaussian prescription.

We only show the case of pn scattering, because its contribution is more important for the neutron-rich isotopes than pp scattering, and also because, as we have discussed in Sec. V, the pn reaction dominates the proton-nucleus reaction cross sections especially at energies less than 100 AMeV.

In Fig. 10, the numerical results of the pn elastic scattering differential cross sections calculated using the parameters of Ref. [20] are compared with the data. The numerical results of the single Gaussian are shown by

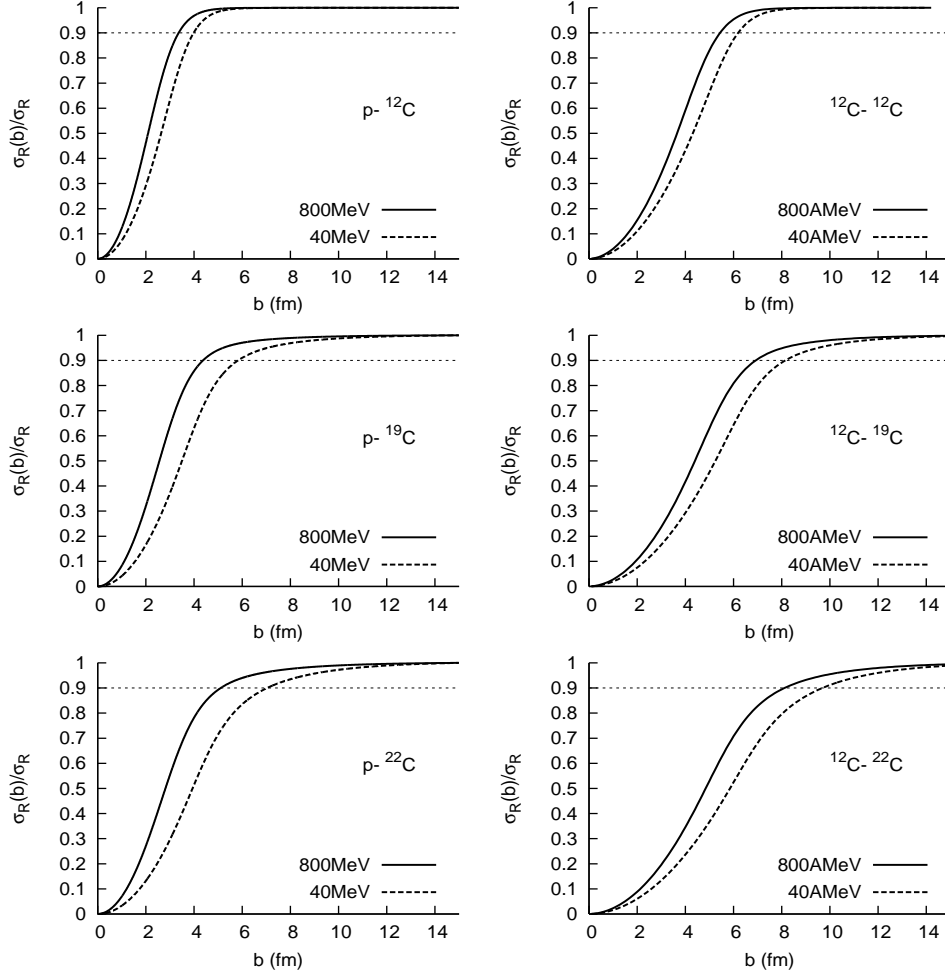


FIG. 9: Comparison of the calculated reaction cross section at a given impact parameter, b , in ratio to the total reaction cross section between proton- $^{12,19,22}\text{C}$ and ^{12}C - $^{12,19,22}\text{C}$. The solid curve is the calculation at 800 MeV, while the dashed curve is at 40 MeV. The dotted line indicates 90 % of σ_R .

the dashed curve. The agreement of the results with the data is reasonable, but not perfect especially in the forward direction.

Although the agreement with the data of the pn elastic differential cross section is imperfect, the expression of the single Gaussian well reproduces the reaction cross sections as in Table VI.

For comparison, we perform fittings for the pn elastic scattering data in the energy range from 40 MeV to 100 MeV, using the parameterization of double Gaussians. For this case, the profile function, Γ_{pN}^D , for pp and pn scatterings, is parameterized in the form

$$\Gamma_{pN}^D(\mathbf{b}) = \frac{1 - i\alpha_1}{4\pi\beta_1} \sigma_1 e^{-b^2/(2\beta_1)} + \frac{1 - i\alpha_2}{4\pi\beta_2} \sigma_2 e^{-b^2/(2\beta_2)}, \quad (18)$$

where, σ_1 , α_1 , β_1 , σ_2 , α_2 and β_2 are fitting parameters determined from the requirement: 1) The optical theorem is satisfied. 2) The ratio of the real to the imaginary part of the $pn(pp)$ scattering amplitude in the forward direction reproduces the experimental values. 3) The to-

tal elastic scattering cross section is equal to the total cross section. 4) The elastic scattering differential cross sections are reproduced.

The fitting results using the double Gaussians are displayed by the solid curves in Fig. 10. The two sets of experimental data shown as 60 MeV in Fig. 10 are at 62 MeV (open circle) and 63 MeV (thick dot). As for the differential cross sections, it seems that the double Gaussians give better results.

In Table VI, we compare the numerical results of proton- ^{12}C total reaction cross sections. The calculations using the double Gaussians are the fit, while those using the single Gaussian are obtained by the use of the parameters of Ref. [20]. The parameters of pp scattering are kept fixed. The experimental data are also shown in the table. The difference between the results of the reaction cross sections using these two parameterizations is a few % except at 60 MeV, but around this energy the data scatter widely and the difference between the numerical results and the data is not serious.

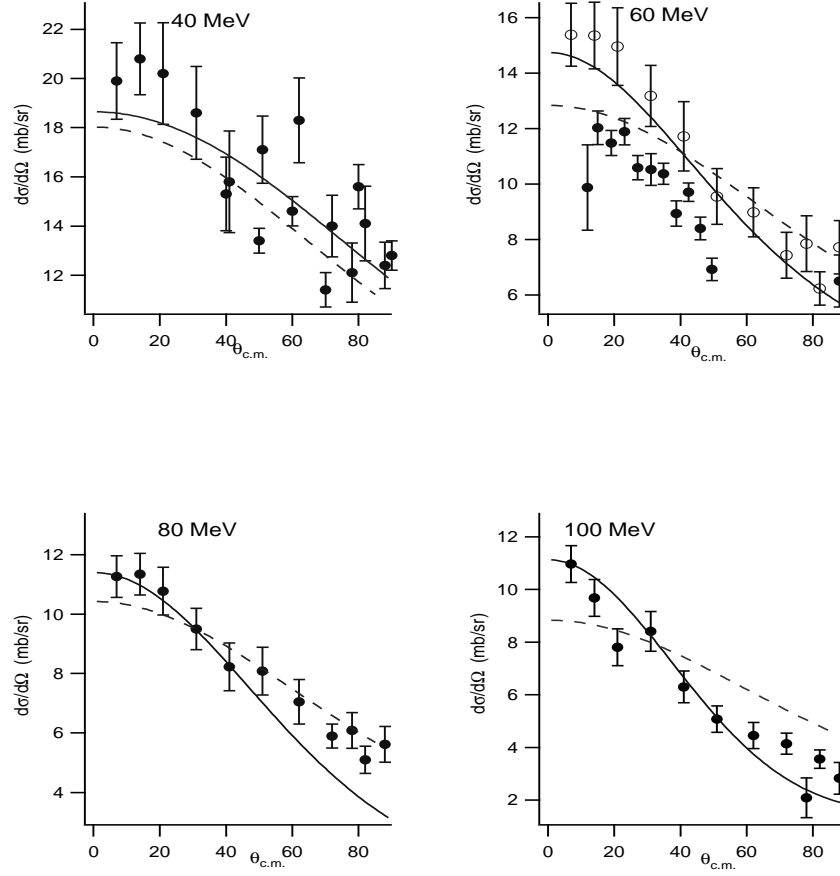


FIG. 10: The differential cross sections of the pn elastic scattering. The solid curves denote the fitting using double Gaussians, as explained in the text, while the dashed curves the results with the parameters listed in Table I. The experimental data are taken from Ref. [28].

TABLE VI: Total reaction cross sections of proton- ^{12}C in mb calculated using the parameters given in Table I, and that determined from two Gaussian fitting for pn elastic scattering data. The experimental data are taken from Refs. [26, 27].

E (MeV)	Table I present fit		Exp.
40	432	416	371(11), 405(38)
60	359	387	310 (13)
80	314	320	279 (10)
100	284	294	275 (21)

Thus, we conclude that the parameters listed in Table I works fairly well for the reaction cross sections. For simplicity, we adopt the parameterization with the single Gaussian throughout this paper.

[1] K. Amos, W.A. Richter, S. Karataglidis, and B.A. Brown, Phys. Rev. Lett. **96**, 032503 (2006).
[2] A. Kohama, R. Seki, A. Arima, and S. Yamaji, J. Phys. Soc. Japan **72**, 2766 (2003).
[3] N. Imai, H.J. Ong, N. Aoi, H. Sakurai, K. Demichi *et al.*, Phys. Rev. Lett. **92**, 062501 (2004).
[4] T. Yamaguchi, T. Zheng, A. Ozawa, M. Chiba, R. Ka-

nungo *et al.*, Nucl. Phys. **A724**, 3 (2003).
[5] T. Nakamura, N. Fukuda, T. Kobayashi, N. Aoi, H. Iwasaki, *et al.*, Phys. Rev. Lett. **83**, 1112 (1999).
[6] V. Maddalena, T. Aumann, D. Bazin, B.A. Brown, J.A. Caggiano *et al.*, Phys. Rev. C **63**, 024613 (2001).
[7] Y. Suzuki, H. Matsumura, and B. Abu-Ibrahim, Phys. Rev. C **70**, 051302(R) (2004).

- [8] W. Horiuchi and Y. Suzuki, Phys. Rev. C **73**, 037304 (2006); Erratum: *ibid.* C **74**, 019901(E) (2006).
- [9] N. Itagaki, T. Otsuka, K. Ikeda and S. Okabe, Phys. Rev. Lett. **92**, 142501 (2004).
- [10] Y. Kanada-En'yo, Phys. Rev. C **71**, 014310 (2005).
- [11] H. Sagawa, X.R. Zhou, X.Z. Zhang, and T. Suzuki, Phys. Rev. C **70**, 054316 (2004).
- [12] W. Horiuchi and Y. Suzuki, Phys. Rev. C **74**, 034311 (2006).
- [13] K. Tanaka *et al.*, QW-005 in *INPC2007 Abstracts* and private communication.
- [14] W. Horiuchi, Y. Suzuki, B. Abu-Ibrahim, and A. Kohama, Phys. Rev. C **75**, 044607 (2007); Erratum: *ibid.* C **76**, 039903(E) (2007).
- [15] R.J. Glauber, in *Lectures in Theoretical Physics* (Interscience, New York, 1959), Vol. 1, p.315.
- [16] K. Yabana, Y. Ogawa, and Y. Suzuki, Nucl. Phys. **A539**, 295 (1992).
- [17] Y. Ogawa, K. Yabana, and Y. Suzuki, Nucl. Phys. **A543**, 722 (1992).
- [18] B. Abu-Ibrahim, Y. Ogawa, Y. Suzuki, and I. Tanihata, Comp. Phys. Commun. **151**, 369 (2003).
- [19] J.S. Al-Khalili and J.A. Tostevin, Phys. Rev. Lett. **76**, 3903 (1996).
J.S. Al-Khalili, J.A. Tostevin and I.J. Thompson, Phys. Rev. C **54**, 1843 (1996).
- [20] J.Y. Hostachy, Thèse d'Etat, I.S.N. 87-65, Université de Grenoble, unpublished.
- [21] L. Ray, Phys. Rev. C **20**, 1857 (1979).
- [22] Particle Data Group, J. Phys. G: Nuclear and Particle Physics, **33**, 1 (2006).
- [23] B. Abu-Ibrahim and Y. Suzuki, Nucl. Phys. **A728**, 118 (2003).
- [24] G. Audi, A.H. Wapstra, and C. Thibault, Nucl. Phys. **A729**, 337 (2003).
- [25] A. Kohama, K. Iida, and K. Oyamatsu, Phys. Rev. C **72**, 024602 (2005).
- [26] R.F. Carlson, Atomic Data and Nuclear Data Tables **63**, 93 (1996).
- [27] A. Auce, A. Ingemarsson, R. Johansson, M. Lantz, G. Tibel *et. al*, Phys. Rev. C **71**, 064606 (2005).
- [28] J.P. Scanlon, G.H. Stafford, J.J. Thresher, and P.H. Bowen, Nucl. Phys. **41**, 401 (1963).